Inorganic Chemistry

Article

pubs.acs.org/IC

Lewis Acid Enhanced Axial Ligation of $[Mo_2]^{4+}$ Complexes

Brian S. Dolinar and John F. Berry*

Department of Chemistry, University of Wisconsin—Madison, 1101 University Avenue, Madison, Wisconsin 53706, United States

Supporting Information

ABSTRACT: We report here the syntheses, X-ray crystal structures, electrochemistry, and density functional theory (DFT) single-point calculations of three new complexes: tetrakis(monothiosuccinimidato)dimolybdenum(II) [$Mo_2(SNO5)_4$, **1a**], tetrakis(6-thioxo-2-piperidinonato)dimolybdenum(II) [$Mo_2(SNO6)_4$, **1b**], and chlorotetrakis(monothiosuccinimidato)-pyridinelithiumdimolybdenum(II) [$pyLiMo_2(SNO5)_4Cl$, **2-py**]. X-ray crystallography shows unusually short axial Mo_2−Cl bond lengths in **2-py**, 2.6533(6) Å, and dimeric **2-dim**, 2.644(1) Å, which we propose result from an increased Lewis acidity of the Mo_2 unit in the presence of the proximal Li^+ ion. When **2-py** is dissolved in MeCN, the lithium reversibly dissociates, forming an equilibrium mixture of ($MeCNLiMo_2(SNO5)_4Cl$) (**2-MeCN**) and $[Li(MeCN)_4]^+[Mo_2(SNO5)_4Cl]^-$ (**3**). Cyclic voltammetry was used to determine the equilibrium lithium binding constant (room temperature, K_{eq} = 95 ± 1). From analysis of the temperature dependence of the equilibrium constant, thermodynamic parameters for the formation of **2-MeCN** from **3** ($\Delta H°$ = −6.96 ± 0.93 kJ mol^{-1} and $\Delta S°$ = 13.9 ± 3.5 J mol^{-1} K^{-1}) were extracted. DFT calculations indicate that Li^+ affects the Mo−Cl bond length through polarization of metal−metal bonding/antibonding molecular orbitals when lithium and chloride are added to the dimolybdenum core.

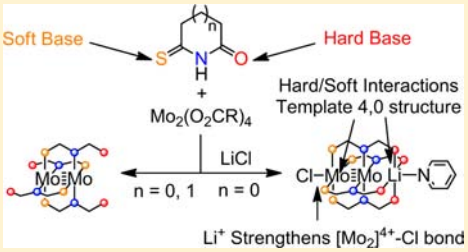

INTRODUCTION

Metal−metal-bonded compounds having the paddlewheel-type structure, shown in Chart 1a, have played a major role in the development of coordination chemistry[1] and continue to be of interest for their catalytic,[2] photophysical,[3] electronic,[4] and structural properties[5] as well as reactivity.[6] The reactivity of ligands in the axial position of these complexes is very important and plays a key role in applications such as catalysis. Only a few $[Mo_2]^{4+}$ compounds are known that are axially ligated with either neutral ligands, such as tetrahydrofuran, nitriles, and a pyrazole derivative,[7] or with anionic ligands, including Cl^-, Br^-, I^-, and $[BF_4]^-$.[8] Dimolybdenum carboxylates can also associate through intermolecular axial interactions with O atoms from an adjacent molecule.[9] In all of these cases, however, these axial ligands are bound exceptionally weakly, with Mo−L_{ax} bond lengths often up to 0.4−0.6 Å longer than their corresponding Mo−L_{eq} bond lengths; more often, $[Mo_2]^{4+}$ complexes eschew axial ligands entirely. Thus, new strategies for the axial functionalization of $[Mo_2]^{4+}$ complexes are of interest.

Chart 1. (a) Paddlewheel-Type Structure Supported by Bridging Anionic Equatorial Ligands $[X-Y-Z]^-$[a] and (b) Qualitative MO Diagram of Metal−Metal Interactions for $[Mo_2]^{4+}$

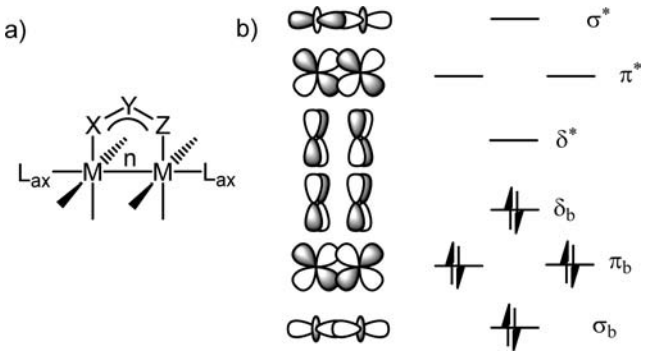

[a]The metal−metal bond order, *n*, can range from 0 to 4, and L_{ax} are axial donor ligands.

The indifference of the $[Mo_2]^{4+}$ unit toward axial ligands has its origin in the electronic structure of the Mo_2 unit. Chart 1b depicts a qualitative molecular orbital (MO) diagram of a $[Mo_2]^{4+}$ species. The principal empty Mo-centered orbital that would have the correct symmetry to overlap with a σ-type lone-pair orbital on a Lewis base is the Mo−Mo σ* orbital. This σ* orbital is elevated in energy by the strong interaction between the d_{z^2} orbitals of the two Mo atoms, resulting in poor energetic matching and, hence, poor overlap with ligand-based σ-type lone-pair orbitals. Thus, axial ligands bind weakly to Mo_2 complexes.

Because of our interest in the reactivity of M_2 complexes, we wanted to see if it were possible to increase the Lewis acidity of Mo_2 species and strengthen Mo_2−axial ligand bonding. An attractive approach to this would be to design complexes that bring a Lewis acid into close proximity with the Mo_2 unit, thus activating it and making it more susceptible to attack by a Lewis base. A similar strategy was recently explored by the Gabbaï

Received: February 1, 2013
Published: March 29, 2013

   dx.doi.org/10.1021/ic400275x | *Inorg. Chem.* 2013, 52, 4658−4667

group, in which inert Hg^{2+} and Au^{+} ions were activated by conjoining them to a proximal Lewis acidic Ar_4Sb^{+} ion, resulting in further ligation of these metals.[10] Also, the Thomas group has recently demonstrated that Lewis acidic Zr^{4+} ions can activate Co^{+}, yielding a complex capable of splitting C═O bonds in CO_2.[11]

With regards to Lewis acid activation of Mo_2 systems, the closest examples were reported by our group on linear heterotrinuclear Mo≡Mo···M complexes using either Co^{2+} or Fe^{2+}, in which chloride ligands bind the open Mo_2 axial position, resulting in Mo−Cl bond distances significantly shorter than those of unactivated Mo_2^{4+} units.[8g,h] We hypothesized, therefore, that stronger Lewis acids, such as alkali metals, should result in more Lewis acidic Mo_2 units and stronger bonds between Mo and axial ligands.

In order to promote the formation of such complexes, a new type of ligand capable of forming trimetallic complexes was designed. As opposed to dipyridylamine ligands used in our earlier Mo≡Mo···M work, which have three nitrogen bases, we have designed a ligand containing a combination of hard and soft bases so that hard−soft acid−base (HSAB) theory could be used to design heterometallic compounds with element-specific structures. Alkoxyalkylphosphines,[12] phosphinoamides,[11,13] and thiopyridines[14] have been used to synthesize heterometallic complexes using a similar concept. Monothiosuccinimide (HSNO5) and 6-thioxo-2-piperidinone (HSNO6), shown in Chart 2, are two ligands that are ideal for this type of chemistry.

Chart 2. Ligands Monothiosuccinimide and 6-Thioxo-2-piperidinone

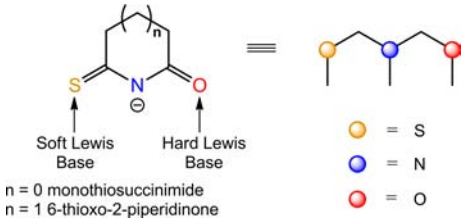

These two ligands differ only in their ring size, and they incorporate hard and soft bases that would facilitate the syntheses of a heterometallic complex containing a hard Lewis acidic fragment and a $[Mo_2]^{4+}$ unit. The sulfur on this ligand is a soft base, and it is able to effectively bind molybdenum, while the oxygen is a hard base, making it ideal to bind alkali ions.

Herein we report the syntheses and characterization of two unactivated dimolybdenum complexes, $Mo_2(SNO5)_4$ (**1a**) and $Mo_2(SNO6)_4$ (**1b**), and a dimolybdenum complex that is activated by the presence of a Lewis acidic lithium cation, $pyLiMo_2(SNO5)_4Cl$ (**2-py**). These complexes (Scheme 1a) have been structurally characterized by X-ray crystallography. We also provide electrochemical evidence that **2-py** reversibly dissociates Li^{+} when dissolved in acetonitrile (MeCN) to form $MeCNLiMo_2(SNO5)_4Cl$ (**2-MeCN**) in equilibrium with $[Li(MeCN)_4]^{+}[Mo_2(SNO5)_4Cl]^{-}$ (**3**; Scheme 1b). To gain more insight into the electronic structure of this complex, density functional theory (DFT) geometry optimizations and single-point calculations were performed on these complexes.

EXPERIMENTAL SECTION

General Procedures. All synthetic manipulations were carried out under an inert N_2 atmosphere using standard Schlenk and glovebox techniques unless otherwise stated. CH_2Cl_2 and $C_2H_4Cl_2$ were dried

Scheme 1. (a) Synthesis Pathway for Forming *trans*-2,2-$Mo_2(SNOX)_4$ Complexes as well as 2-py and (b) Proposed Equilibrium Involving Li^{+} Dissociation from Compound 2-MeCN

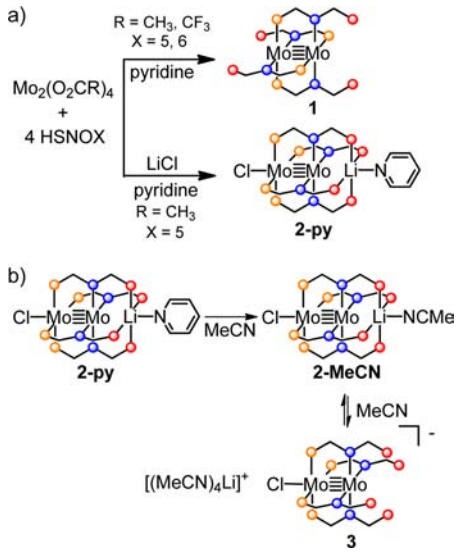

sequentially over molecular sieves and CaH_2 and distilled under N_2 prior to use. Tetrahydrofuran (THF) was dried using a Vacuum Atmospheres solvent purification system and degassed with N_2 prior to use. Pyridine was dried sequentially over molecular sieves and barium oxide. It was then distilled under N_2 and stored in a glovebox prior to use. All other commercial reagents were used as received without further purification. Lawesson's reagent, glutarimide, succinimide, P_2S_5, lithium hexafluorophosphate, tetrabutylammonium hexafluorophosphate, trifluoroacetic acid, acetic acid, and molybdenum carbonyl were purchased from Sigma Aldrich. Molybdenum acetate $[Mo_2(OAc)_4]$ was synthesized from molybdenum carbonyl and acetic acid.[15] Molybdenum trifluoroacetate $[Mo_2(TFA)_4]$ was synthesized from $Mo_2(OAc)_4$ and trifluoroacetic acid.[16] Monothiosuccinimide (HSNO5) was prepared from succinimide and P_2S_5.[17] 6-Thioxo-2-piperidinone (HSNO6) was prepared from glutarimide and Lawesson's reagent.[18] Elemental analysis was carried out by Midwest Microlabs in Indianapolis, IN. Mass spectrometry data were recorded at the Mass Spectrometry Facility of the Chemical Instrument Center of the University of Wisconsin—Madison. Matrix-assisted laser desorption/ionization mass spectrometry (MALDI-MS) spectra were obtained using a Bruker REFLEX II spectrometer equipped with a 337 nm laser, a reflectron, delayed extraction, and a time-of-flight analyzer. The acceleration voltage was 25 kV. IR spectra were taken on a Bruker TENSOR 27 using ATR techniques. ^{1}H NMR spectra were recorded on a Bruker AC+ 300 spectrometer. ^{13}C and ^{7}Li NMR spectra were recorded on a Bruker Avance-500 spectrometer.

*trans-2,2-Tetrakis(monothiosuccinimidato)dimolybdenum(II) ($Mo_2(SNO5)_4$, **1a**).* A flask was charged with 246 mg of HSNO5 (2.14 mmol), 331 mg of $Mo_2(TFA)_4$ (0.521 mmol), and 30 mL of pyridine. The resulting reaction mixture was heated to reflux with stirring for 3 h. The reaction mixture was then allowed to cool to room temperature, and the solvent was removed under vacuum. The resulting residue was washed with 3 × 20 mL of Et_2O. This gave an orange-brown powder, which was extracted with 20 mL of hot CH_2Cl_2. Layering this extract with hexanes gave **1a** as a brown powder. The solid was filtered in air and washed with 3 × 20 mL of hexanes and 1 × 20 mL of Et_2O. Yield: 199 mg (59.0%). ^{1}H NMR (300 MHz, $CDCl_3$): δ 3.563 (m, 8H), 2.885 (m, 8H). ^{13}C NMR (500 MHz, $CDCl_3$): δ 215.85, 215.57, 186.91, 186.58, 39.55, 32.30. (The doubling of the signals at 215 and 186 ppm is likely due to the presence of multiple conformers in solution.) MALDI-MS (**1a**$^{+}$): m/z 651. IR (ATR, cm^{-1}): 1755 w, 1725 m, 1438 m, 1415, m, 1398 m, 1248 m, 1191 vs, 990 vw, 963 w, 917 m, 804 m, 733 m. UV−vis (CH_2Cl_2, λ

dx.doi.org/10.1021/ic400275x | Inorg. Chem. 2013, 52, 4658−4667

Table 1. X-ray Crystallographic Solution Details for Compounds 1 and 2-py

	1a	1b	2-py	2-dim
empirical formula	$C_{16}H_{16}Mo_2N_4O_4S_4$	$C_{23}H_{30}N_4O_4S_4Cl_3Mo_2$	$C_{26}H_{26}LiN_6O_4S_4ClMo_2$	$C_{34}H_{36}Cl_6Li_2Mo_4N_8O_8S_8$
fw	648.45	852.98	849.04	1551.53
temperature/K	100(1)	100(1)	100(1)	100(1)
λ/Å	1.54178	0.71073	0.71073	0.71073
cryst syst	orthorhombic	monoclinic	orthorhombic	monoclinic
space group	*Pccn*	$P2_1/n$	$P2_12_12_1$	$P2_1/n$
a/Å	10.6032(7)	10.6871(3)	8.6895(3)	8.704(3)
b/Å	12.591(1)	19.8411(6)	13.7221(5)	22.530(8)
c/Å	15.842(2)	15.3151(5)	26.1281(9)	13.543(5)
β/deg	90	106.159(1)	90	108.07(2)
volume/Å^3	2115.0(3)	3119.2(2)	3115.5(2)	2525(2)
Z	4	4	4	2
ρ_{calc}/mg mm^{-3}	2.036	1.816	1.810	2.041
final R indexes[a] [$I \geq 2\sigma(I)$]	R1 = 0.0271, wR2 = 0.0733	R1 = 0.0290, wR2 = 0.0664	R1 = 0.0186, wR2 = 0.0381	R1 = 0.0309, wR2 = 0.0621
final R indexes [all data]	R1 = 0.0281, wR2 = 0.0741	R1 = 0.0389, wR2 = 0.0709	R1 = 0.0204, wR2 = 0.0387	R1 = 0.0504, wR2 = 0.0683
Flack Parameter			−0.03(2)	

[a] $R1 = 3||F_o| - |F_c||/[3|F_o|]$. $wR2 = \{3[w(F_o^2 - F_c^2)^2]/[3[w(F_o^2)^2]]\}^{1/2}$, $w = 1/\sigma^2(F_o^2) + (aP)^2 + bP$, where $P = [\max(0 \text{ or } F_o^2) + 2(F_c^2)]/3$.

(nm) [ε (M^{-1} cm^{-1})]): 414 [5400], 495 [830]. Elem anal. Calcd for $C_{16}H_{16}S_4N_4O_4Mo_2$ (**1a**): C, 29.63; H, 2.49; N, 8.64. Found: C, 29.64; H, 2.57; N, 7.96.

*trans-2,2-Tetrakis(6-thioxo-2-piperidinonato)dimolybdenum(II) (Mo_2(SNO6)$_4$, **1b**).* A flask was charged with 320 mg of HSNO6 (2.48 mmol), 264 mg of $Mo_2(OAc)_4$ (0.572 mmol), 148 mg of LiCl, and 15 mL of pyridine, and the resulting reaction mixture was heated to reflux with stirring for 16 h. The solvent was then removed under vacuum, leaving a red oily residue. The residue was triturated with 2 × 15 mL of Et_2O, yielding a fine red solid. The solid was extracted with 20 mL of 1,2-dichloroethane, and crystals were grown from the resulting solution by layering with 80 mL of hexanes. Compound **1b** was isolated by filtration as a red microcrystalline solid. Yield: 201 mg (46.2%). ^{1}H NMR (300 MHz, $CDCl_3$): δ 3.325 (t, J = 6 Hz, 8H), 2.521 (t, J = 6.6 Hz, 8H), 2.156 (p, J = 6.3 Hz, 8H). ^{13}C (500 MHz, $CDCl_3$): δ 207.96, 177.53, 39.13, 31.69, 21.86. MALDI-MS (**1b**$^+$): m/z 705. IR (ATR, cm^{-1}) 2959 vw, 1675 m, 1604 w, 1521 w, 1485 w, 1441 s, 1407 s, 1333 m, 1323 m, 1261 vs, 1245 vs, 1181 vs, 1115 vs, 1070 w, 1042 w, 1012 w, 975 m, 962 m, 912 m, 846 w, 758 m, 677 s, 651 s. UV−vis (THF, λ (nm) [ε (M^{-1} cm^{-1})]): 460 [12000]. Elem anal. Calcd for $C_{20}H_{24}S_4N_4O_4Mo_2$ (**1b**): C, 34.09; H, 3.43; N, 7.95. Found: C, 34.03; H, 3.41; N, 7.84.

*4,0-Chlorotetrakis(monothiosuccinimidato)-pyridinelithiumdimolybdenum(II) (pyLiMo_2(SNO5)$_4$Cl, **2-py**).* A flask was charged with 326 mg of HSNO5 (2.83 mmol), 303 mg of $Mo_2(OAc)_4$ (0.706 mmol), and 320 mg of LiCl (7.6 mmol) dissolved in 20 mL of pyridine. The resulting solution was heated to 100 °C without stirring. Within a few hours, red-orange crystalline **2-py** began to precipitate from the solution. After 16 h, the reaction was cooled to room temperature. Compound **2-py** was collected by filtration, washed with 3 × 20 mL of THF and 2 × 20 mL of hexanes, and dried under vacuum. Yield: 369 mg (61.6%). ^{1}H NMR (300 MHz, MeCN-d^3): δ 8.59 (m, 2H), 7.745 (tt, J = 7.8 and 1.8 Hz, 1H), 7.34 (m, 2H), 3.58 (m, 8H), 2.78 (m, 8H). ^{13}C NMR (500 MHz, MeCN-d^3): δ 192.73, 150.76, 137.04, 124.83, 95.74, 41.29, 33.39. ^{7}Li NMR (500 MHz, DMF): δ 0.547. IR (ATR, cm^{-1}): 2963 vw, 1724 m, 1569 vw, 1441 w 1429 w, 1390 w, 1259 s, 1236 s, 1217 s, 1086 m, 1034 s, 1018 s, 962 w, 937 w, 863 w, 797 vs, 753 w, 703 m, 684 m, 665 m, 629 w. UV−vis (MeCN, λ (nm) [ε (M^{-1} cm^{-1})]): 433 [5300], 521 [530]. Elem anal. Calcd for $C_{26}H_{26}N_6S_4O_4Mo_2Li$ (**2-py**·py): C, 36.78; H, 3.09; N, 9.90. Found: C, 36.64; H, 3.09; N, 9.80.

X-ray-quality crystals of dimeric $[LiMo_2(SNO5)_4Cl]_2$ (**2-dim**) were also obtained by crystallizing **2-py** from CH_2Cl_2/py/hexanes.

X-ray Crystallography. Suitable crystals of **1a**, **1b**, **2-py**, and **2-dim** were selected under oil and ambient conditions. For **1a**, an orange plate-shaped single crystal with dimensions 0.118 × 0.087 × 0.075 mm^3 was selected. For **1b**, an orange-yellow block-shaped crystal with dimensions 0.370 × 0.190 × 0.090 mm^3 was selected. For **2-py**, a red plate-shaped crystal with dimensions 0.210 × 0.184 × 0.029 mm^3 was selected. For **2-dim**, an orange rod-shaped crystal with dimensions 0.100 × 0.050 × 0.030 mm^3 was selected. Crystals were attached to the tip of a MiTeGen MicroMount, mounted in a stream of cold nitrogen at 100(1) K, and centered in the X-ray beam using a video monitoring system. Crystal evaluation and data collection were performed on a Bruker Quazar SMART APEX-II diffractometer with Cu Kα (λ = 1.54178 Å; **1a**) or Mo Kα (λ = 0.71073 Å; **1b**, **2-py**, and **2-dim**) radiation. The data were collected using a routine to survey an entire sphere of reciprocal space and indexed by the *SMART* program, and the structures were solved via direct methods and refined by iterative cycles of least-squares refinement on F^2 followed by difference Fourier synthesis.[19] All H atoms were included in the final structure factor calculation at idealized positions and allowed to ride on the neighboring atoms with relative isotropic displacement coefficients.

The details concerning X-ray crystallographic solutions and refinement for compounds **1a**, **1b**, and **2-py** are tabulated in Table 1. For each structure, the model was refined to a low wR2 value (<0.10 for each case). After refinement of the model, compound **2-py** had a featureless final Fourier map. For compounds **1a** and **1b**, the final Fourier maps had peaks of 1.34 and 1.36 e Å^{-3}, respectively. These highest peaks were located closest to the heaviest atoms in the models (Mo) and were interpreted as noise. For compound **2-py**, the absolute structure was established by anomalous dispersion using the method of Flack.[20]

Electrochemistry. Compounds **2-MeCN** and **3** were prepared in situ by dissolving **2-py** in a 100 mM solution of NBu_4PF_6 in MeCN at room temperature under ambient conditions and subsequently titrating the solution with either $LiPF_6$ or 12-crown-4 ether, respectively. Cyclic voltammetry for compounds **1a**, **1b**, **2-MeCN**, and **3** was performed on solutions of 1 mM analyte and 100 mM electrolyte (NBu_4PF_6) at temperatures ranging from −29 to +20 °C using a standard glassy carbon electrode as the working electrode, a platinum wire as the auxiliary electrode, and Ag/Ag$^+$ as the reference electrode. All electrochemical potentials were internally referenced to the ferrocene/ferrocenium (Fc/Fc$^+$) couple. The voltammetry was performed in the range of +900 to −500 mV for compounds **2-MeCN** and **3** or to −1700 mV for compounds **1a** and **1b** at a scan rate of 100 mV s^{-1}. The solvents used were MeCN for compounds **1a**, **2-MeCN**, and **3** and CH_2Cl_2 for compound **1b**.

DFT Calculations. Restricted Kohn−Sham geometry optimization and single-point calculations were carried out on **1a** and **2-py** through the ORCA calculation package using the BP86 functional.[21] The def2-TZVP (Mo and Cl atoms) and def2-SVP (all other atoms) basis sets from the Karlsruhe group,[22] which are automatically recontracted in ORCA for use with the scalar relativistic zeroth-order regular

dx.doi.org/10.1021/ic400275x | Inorg. Chem. 2013, 52, 4658−4667

Table 2. Important Bond Distances and Bond Angles for the X-ray Crystal Structures of Compounds 1a, 1b, 2-py, and 2-dim

	$Mo_2(SNO5)_4$ (1a)	$Mo_2(SNO6)_4$ (1b)	$pyLiMo_2(SNO5)_4Cl$ (2-py)	$[LiMo_2(SNO5)_4Cl]_2$ (2-dim)
D(Mo−Mo) (Å)	2.1112(4)	2.1150(2)	2.1357(3)	2.1354(8)
D(Mo−N) (Å)	2.145[2]	2.153[3]	2.119[2]	2.123[3]
D(Mo−S) (Å)	2.4753[8]	2.481[8]	2.5172[6]	2.514[1]
D(Mo−Cl) (Å)			2.6533(6)	2.644(1)
$D(Li-O)_{eq}$ (Å)			2.182[6]	2.185[7]
D(Li···Mo) (Å)			3.075(5)	3.049(6)
A(Mo−Mo−Cl) (deg)			176.24(2)	174.95(2)
A(Li−Mo−Mo) (deg)			178.7(1)	177.3(1)

approximation (ZORA), were used. Structures for compounds **1a** and **2-py** were calculated using initial atomic coordinates taken from the crystal structures and then optimized until the energy change between steps was less than 10^{-6} hartree. All calculations were optimized with a Grid4 optimization grid and tight self-consistent-field convergence criteria.

RESULTS AND DISCUSSION

Synthesis. Compounds **1a** and **1b** were synthesized in useful yields by reacting free HSNO5 and HSNO6 ligands with $Mo_2(TFA)_4$ and $Mo_2(OAc)_4$, respectively, under N_2 in refluxing pyridine. For these reactions, pyridine serves two purposes. First, it is a solvent with a high boiling point (~130 °C at 1.1 bar), so the reactions can be heated to a high enough temperature to proceed to completion. Second, the basicity of pyridine drives this reaction by removing the acetic or trifluoroacetic acid formed via ligand substitution.

Lithium chloride is an important additive that aids in the purification of **1b**. The pyridinium acetate byproduct formed in the reaction is not soluble in Et_2O or hexanes, but it is soluble in 1,2-dichloroethane and CH_2Cl_2, as is **1b**. When LiCl is added to the reaction, lithium acetate and pyridinium chloride are formed instead of pyridinium acetate, and so the purification of **1b** can be accomplished by washing the mixture with Et_2O and subsequent extraction with 1,2-dichloroethane because now only **1b** is soluble in this solvent. When LiCl is not added to the reaction mixture, only an impure, noncrystalline product can be obtained from the reaction. Both compounds **1a** and **1b** are somewhat air-stable under ambient conditions, but they degrade slowly after exposure to air and moisture over the course of several months.

Compound **2-py** is the product of the reaction of $Mo_2(OAc)_4$ with HSNO5 and excess LiCl under N_2 in hot pyridine (100 °C). The product precipitates from pyridine, greatly simplifying workup and leading to good yields (61.6%). Like **1a** and **1b**, **2-py** is similarly air- and moisture-stable. **2-py** is sparingly soluble in most noncoordinating solvents such as dichloromethane and toluene, but it is more soluble in strongly coordinating solvents such as dimethyl sulfoxide, MeCN, pyridine, and *N*,*N*-dimethylformamide (DMF). The lithium-bound pyridine ligand in **2-py** is labile. Simple recrystallization of **2-py** from a mixture of CH_2Cl_2 and pyridine affords **2-dim**, in which the py ligand is lost and replaced by an intermolecular Li−O interaction with an O atom from an adjoining $LiMo_2(SNO5)_4Cl$ species. When **2-py** is dissolved in coordinating solvents, it is assumed that the donor solvent replaces the py ligand. **2-py** can also be delithiated, as evidenced by the electrochemistry of **2-py** in MeCN (vide infra). In solution, the lithiated and nonlithiated species are in equilibrium, as illustrated in Scheme 1b.

Synthesis of the HSNO6 complex analogous to **2-py** $[pyLiMo_2(SNO6)_4Cl]$ was attempted as well, and $Li-Mo_2(SNO6)_4Cl$ was obtained but only in very poor yield.[23] Formation of this compound is likely disfavored because of the smaller binding pocket available for Li^+ in complexes of the SNO6 ligand compared with complexes of the SNO5 ligand.

X-ray Crystallography. A list of relevant bond lengths and bond angles for compounds **1a**, **1b**, **2-py**, and **2-dim** described here is included in Table 2.

Compound **1a** crystallized in the orthorhombic space group *Pccn* from the slow diffusion of hexane into a solution of the compound in dichloromethane (Figure 1). The complex has

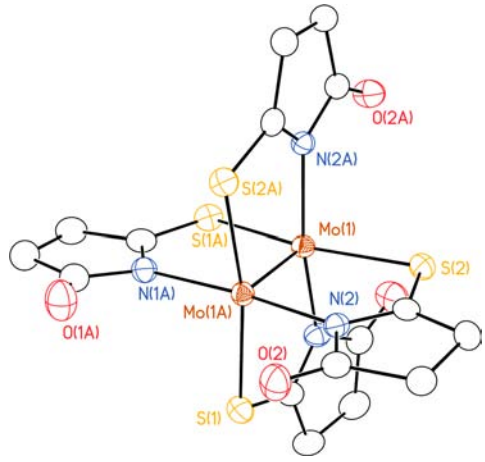

Figure 1. X-ray crystal structure of compound **1a**. All atoms are drawn as 50% thermal probability ellipsoids, and all H atoms are omitted for clarity. The structure of the compound is the *trans*-2,2 isomer.

idealized D_{2d} symmetry, and a crystallographic 2-fold axis bisects the Mo−Mo vector. Following the conventional nomenclature for isomeric paddlewheel-type compounds bridged by ligands bearing two different donor atoms,[1] the *trans*-2,2 isomer of **1a** is observed here. This means that two of the SNO5 ligands are aligned one way along the Mo−Mo bond axis, while the other two ligands are aligned in the opposite direction. Each Mo atom in complex **1a** is, therefore, bound to two S atoms trans to each other and two N atoms trans to each other. The Mo−Mo distance of 2.1112(4) Å is typical of a Mo_2 quadruple bond.[15,16] The Mo−N bond lengths are within the range of reported values for similar dimolybdenum complexes containing four equatorial N−S ligands (2.130−2.199 Å), while the Mo−S bond lengths are slightly longer than the range reported in the literature (2.444−2.468 Å).[24] The sp^2 hybridization of the carbonyl and thioxo C atoms of each ligand in compound **1a** results in the entire SNO5 ligand being planar.

The X-ray crystal structure for **1b** is shown in Figure 2. Compound **1b** crystallizes in the monoclinic space group $P2_1/n$

dx.doi.org/10.1021/ic400275x | Inorg. Chem. 2013, 52, 4658−4667

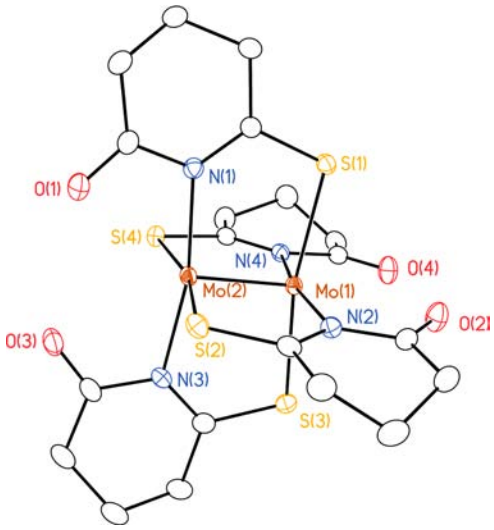

Figure 2. X-ray crystal structure of **1b**. All atoms are drawn as 50% thermal probability ellipsoids, and all H atoms are omitted for clarity. **1b** crystallizes with 1.5 molecules of 1,2-dichloroethane in the asymmetric unit (not shown).

with 1.5 1,2-dichloroethane solvent molecules in the asymmetric unit. Like **1a**, **1b** adopts the *trans*-2,2 configuration. The average Mo−N, Mo−S, and Mo−Mo bond distances are all similar to the corresponding bond distances for **1a**. Unlike the structure of compound **1a**, in **1b**, the six-membered ring of the SNO6 ligand is puckered with the C atom in the 4 position out of the plane of the ligand.

In both compounds **1a** and **1b**, the Mo−N bond distance is significantly shorter than the Mo−S bond distance primarily because of the difference between the atomic radii of the N and S atoms. The difference in these bond lengths, >0.3 Å, results in the ligand being canted, pushing the O atoms of opposite ligands closer together. In **1b**, the nonbonded distance between the O atoms (3.28 Å) is significantly shorter than the distance between the O atoms in **1a** (4.60 Å). In the SNO6 case, steric crowding by the O atoms limits the available space for Li^+ to bind, whereas in the SNO5 case, the O atoms are not nearly as close together, providing a much larger binding pocket to accommodate a Li^+ cation. It is likely that the preference for the *trans*-2,2 configuration also stems from the fact that the O atoms could be too close together in the other possible isomers.

Compound **2-py** crystallizes from the pyridine reaction mixture in the noncentrosymmetric space group $P2_12_12_1$ as a monomer, as shown in Figure 3. The compound also can crystallize from a noncoordinating solvent such as CH_2Cl_2 as a pyridine-free dimer (**2-dim**; Figure 4), which has bond distances and bond angles very similar to those of **2-py**. The crystal structure shows that **2-py** adopts the 4,0 isomer as opposed to the 2,2 isomer of compounds **1a** and **1b**, as well as all previously synthesized $[Mo_2]^{4+}$ complexes with N,S equatorial ligands.[24] Also, unlike **1a** and **1b**, **2-py** contains a coordinated Li^+ ion along the Mo≡Mo axis at a distance of 3.07 Å from the Mo_2 unit. It therefore appears that Li^+ acts as a template for the SNO5 ligands, allowing formation of the 4,0 isomer.

The Mo−Cl distances in **2-py** and **2-dim** are 2.6533(6) and 2.644(1) Å, respectively, which are the shortest distances yet reported for an axial Cl^- ion trans to a Mo≡Mo bond. The Mo−Mo bond distances are 2.1356(3) and 2.1354(8) Å, respectively, which are longer than the Mo−Mo bond distances

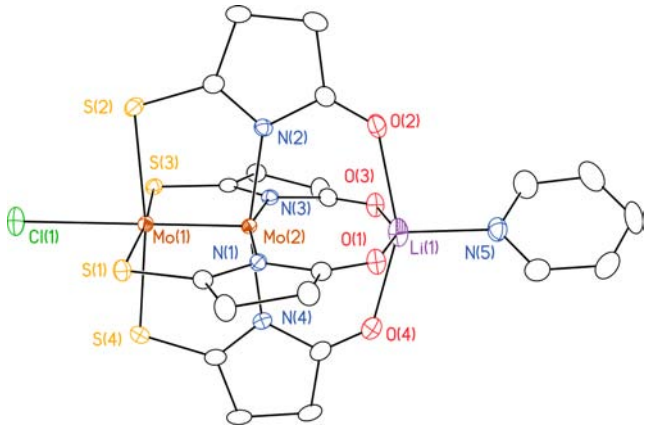

Figure 3. X-ray crystal structure of monomeric **2-py** All atoms are drawn as 50% thermal probability ellipsoids, and all H atoms are omitted for clarity. **2-py** crystallizes with an additional molecule of pyridine in the asymmetric unit (not shown).

Figure 4. X-ray crystal structure of dimeric **2-dim**. All atoms are drawn as 50% thermal probability ellipsoids, and all H atoms are omitted for clarity. **2-dim** crystallizes with two additional molecules of CH_2Cl_2 per dimer (not shown).

in compounds **1a** and **1b** by 0.025 Å. The differences in the Mo−Mo bond distance are statistically significant but may not carry much chemical significance.

A comparison of the axial Mo−Cl bond distances from **2-py** and **2-dim** and those of other known Mo_2−Cl(ax) compounds reported in the CSD is listed in Table 3. The previously synthesized Mo_2 complexes can be divided into two categories: Mo_2 complexes with no additional Lewis acid present and Mo_2 complexes with a late transition metal acting to increase the Mo_2 Lewis acidity. The Mo−Cl bond distances in unactivated $[Mo_2]^{4+}$−Cl complexes range from 2.714(1) to 2.864[2] Å with an average of 2.8242[5] Å. The $[Mo_2]^{4+}$ complexes activated by a late-transition-metal Lewis acid, in general, have shorter Mo−Cl bond lengths [2.720(1) and 2.707(1) Å]. The axial Mo−Cl bond distances in **2-py** and **2-dim** are much shorter than those in either of these classes of compounds. Thus, the increased Lewis acidity of Li^+ activates the $[Mo_2]^{4+}$ core far better than even late transition metals.

dx.doi.org/10.1021/ic400275x | *Inorg. Chem.* 2013, 52, 4658−4667

Table 3. Mo−Mo and Mo−Cl Distances of Unactivated, Late-Transition-Metal-Activated, and Alkali-Metal-Activated $[Mo_2]^{4+}$-Cl Complexes[a]

compound	Mo−Mo (Å)	Mo−Cl (Å)
Unactivated		
$Mo_2(O_2CH)_4KCl$[8a]	2.106[2]	2.864[2]
$Mo_2Cl_2(OAc)_2(\mu\text{-dppa})_2$[8b]	2.152(2)	2.862(3)
$\{[trans\text{-}Mo_2(O_2CCF_3)_2(\mu\text{-dppa})]_3(\mu_6\text{-}CO_3)(\mu\text{-}Cl)_3\}F$[8c]	2.154[1]	2.877[3]
$Mo_2(O_2CC_6H_3(NH_3)_2)_4Cl_8$[8d]	2.107(1)	2.854(2)
$[Pd_2Cl_2(CNC_6H_3Me_2\text{-}2,6)_4][Mo_2(O_2CCF_3)_4]$[8e]	2.1312(3)	2.7747(5)
$Mo_2Cl_2(OAc)_2(\mu\text{-dppma})_2$[8f]	2.1719(8)	2.714(1)
Late-Transition-Metal Activated		
$Mo_2Fe(dpa)_4Cl_2$[8g]	2.168(3)	2.707(1)
$Mo_2Co(dpa)_4Cl_2(CH_2Cl_2)_2$[8h]	2.1027(5)	2.720(1)
Alkali-Metal Activated		
$pyLiMo_2(SNO5)_4Cl$ (**2-py**)	2.1356(3)	2.6533(6)
$[LiMo_2(SNO5)_4Cl]_2$ (**2-dim**)	2.1354(8)	2.644(1)

[a]dppa = *N*,*N*-bis(diphenylphosphino)amine, dppma = *N*,*N*-bis-(diphenylphosphino)methylamine, and dpa = dipyridylamine.

Electrochemistry. Quadruply bonded Mo_2^{4+} compounds can often be oxidized to the corresponding Mo_2^{5+} level in which the Mo−Mo bond order is 3.5.[2,5,6b] The new compounds reported here all show one quasi-reversible wave in their respective cyclic voltammograms (Figure 5), consistent with

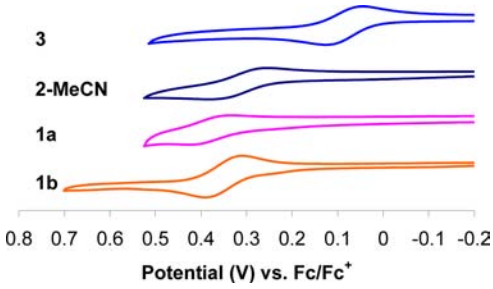

Figure 5. Cyclic voltammograms of compounds **1a** (pink), **1b** (orange), **2-MeCN** (navy), and **3** (blue).

the $Mo_2^{4+/5+}$ redox couple. While **1a** and **1b** show reversible waves at 388 and 351 mV vs Fc/Fc^+, respectively, the redox potential of **2-py** depends strongly on the conditions of the electrochemistry and, most importantly, on the $[Li^+]$ concentration supplied by the supporting electrolyte (Figure 6). For example, a solution of **2-py** in 0.1 M NBu_4PF_6 in MeCN shows a reversible wave at 204 mV, which becomes less accessible as $LiPF_6$ is added to the supporting electrolyte, ultimately reaching a value of 319 mV. If, instead, the strong Li^+ chelating agent 12-crown-4 ether is added to a solution of **2-py**, the $Mo_2^{4+/5+}$ wave becomes drastically more accessible, reaching a plateau at 89 mV. These data are consistent with a Li^+ complexation/decomplexation equilibrium in which the Li^+ ion of **2-py** may be reversibly removed. For the species involved in this equilibrium, we propose the structures **2-MeCN** and **3** (Scheme 2); for the former compound, we make the reasonable assumption that, upon being dissolved in MeCN, the pyridine ligand in **2-py** is quickly replaced with MeCN. For **3**, we hypothesize that the axial Cl^- does not dissociate, which is consistent with the low oxidation potential of the compound.

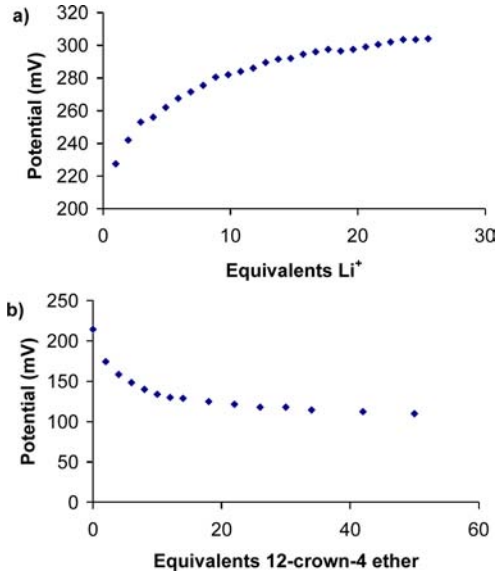

Figure 6. Potential of the MeCN solution of **2-py** as a function of (a) the equivalents of Li^+ added and (b) the equivalents of 12-crown-4 added. All potentials are referenced to the Fc/Fc^+ redox couple.

Scheme 2. Square Scheme for the Electrochemistry of Complexes 2-MeCN and 3

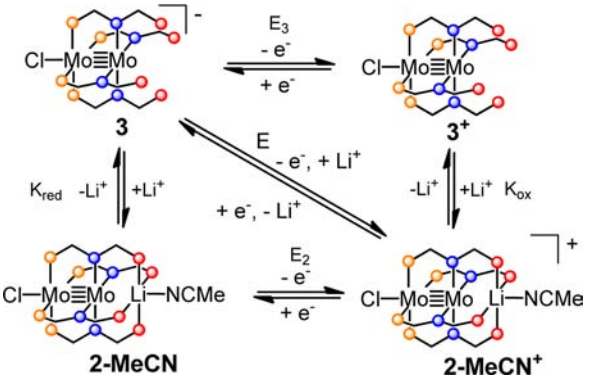

On the basis of the experiments described above, the $Mo_2^{4+/5+}$ potentials of **2-MeCN** and **3** are assigned as shown in Table 4.

Table 4. Electrochemical Potentials for Oxidation of Complexes 1−3 as Well as Other $[Mo_2]^{4+}$ Complexes with N,S Equatorial Ligands[a]

compound	potential vs Fc/Fc^+ (mV)	solvent
$2,2\text{-}Mo_2(SNO5)_4$ (**1a**)	388	MeCN
$2,2\text{-}Mo_2(SNO6)_4$ (**1b**)	351	CH_2Cl_2
4,0-MeCNLiClMo$_2$(SNO5)$_4$ (**2-MeCN**)	319	MeCN
$4,0\text{-}[Mo_2(SNO5)_4Cl]^-$ (**3**)	89	MeCN
$Mo_2(Ph_2PC(S)NMe)_4$[24b]	180	CH_2Cl_2
$Mo_2(Ph_2PC(S)NPh)_4$[24b]	240	CH_2Cl_2
$Mo_2(Me_2NC(S)NMe)_4$[24b]	210	CH_2Cl_2
$Mo_2(\{NPh\}C(S)C{\equiv}CPh)_4$[24e]	92	DMF
	297	THF
Mo_2(2-mercaptoquinoline)$_4$[24c]	520	CH_2Cl_2
	1320	CH_2Cl_2

[a]All potentials are given referenced to the Fc/Fc^+ couple.

dx.doi.org/10.1021/ic400275x | Inorg. Chem. 2013, 52, 4658−4667

Because the metalated and demetalated complexes have different oxidation potentials, this system is an example of metal-coupled electron transfer (MCET).[26] In MCET, the redox potential of a compound behaves according to eqs 1 and 2, which are derived from the Nernst equation using Hess's law.

$$E = E_2 - \frac{RT}{F}[\ln(K_{red})] \quad (1)$$

$$E = E_3 - \frac{RT}{F}[\ln(K_{ox})] \quad (2)$$

Thus, for the **2-MeCN**/**3** equilibrium, the thermodynamics of lithium binding to both **3** and **3**$^+$ can be calculated using the oxidation potentials of pure **2-MeCN** and **3** as well as determining the oxidation potential of an equilibrium mixture of the two and by using the square scheme shown in Scheme 2. At 20 °C, the oxidation potential of a solution of **2-py** in MeCN with no additional Li$^+$ or 12-crown-4 ether added is 204 mV, which corresponds to an equilibrium constant K_{red} = 95 ± 1. The equilibrium constants for lithium binding to the oxidized complex (**3**$^+$) and nonoxidized complex (**3**) were determined at temperatures ranging from −29 to +20 °C. Van't Hoff plots of these equilibrium constants are shown in Figure 7. From these

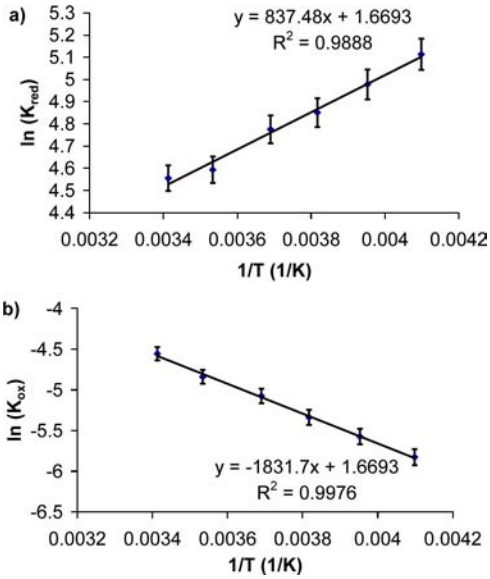

Figure 7. Van't Hoff plots for the equilibrium between (a) **2-MeCN** and **3** and (b) **2-MeCN**$^+$ and **3**$^+$. Equilibrium constants were measured over a range of −29 to +20 °C.

plots, the standard enthalpy and entropy of lithium binding to **3** and **3**$^+$ were determined ($\Delta H°$ = −6.96 ± 0.93 kJ mol^{-1} and $\Delta S°$ = 13.9 ± 3.5 J mol^{-1} K^{-1} for **3** and $\Delta H°$ = 15.2 ± 1.3 kJ mol^{-1} and $\Delta S°$ = 13.9 ± 4.9 J mol^{-1} K^{-1} for **3**$^+$). The positive value for the change in the entropy in both of these cases is sensible. Free Li$^+$ ions in MeCN solution are usually coordinated to four MeCN molecules in a tetrahedral fashion.[27] Binding lithium to **3** will therefore result in the net gain of two molecules in the system, increasing the entropy.

It is useful to compare the data obtained here with the complexation of Li$^+$ with 12-crown-4 ether in MeCN, which yields a 2:1 ligand/Li$^+$ complex. Formation of this complex is entropically disfavored by ∼10 J mol^{-1} K^{-1}.[28] We speculate that the negative entropy of the 12-crown-4 system is largely due to a loss of conformational flexibility of the 12-crown-4 ether upon complexation with Li$^+$. The ligands of **3** are already rigidly held by the $[Mo_2]^{4+}$ unit, eliminating this entropy sink.

Interestingly, the value of ΔH is negative for **3** but positive for **3**$^+$. In binding Li$^+$ to **3**, the compound is stabilized by the hard acid−hard base interaction of the four O atoms and Li$^+$. When Li$^+$ binds to **3**$^+$, it is also stabilized by these same interactions, but it is destabilized to a greater degree by Coulombic repulsion between the increased charge of the Mo_2 core and Li$^+$. This Coulombic repulsion proves to contribute more to the overall enthalpy of the reaction than stabilization by the Lewis acid−Lewis base interactions.

In comparison, the enthalpy of lithium binding to 12-crown-4 ether is more exothermic than lithium binding to **3** by about 17 kJ mol^{-1}.[28] The difference in enthalpy likely stems from the eight total Li−O bonds formed in complexation between 12-crown-4 ether and Li$^+$, as opposed to the four Li−O bonds formed when Li$^+$ binds to **3**.

DFT Calculations. The optimized bond distances and bond angles are shown in Table 5 and compared to the crystal

Table 5. Experimental and Calculated Bond Distances and Bond Angles for 1a and 2-py

	1a exp	**1a** calcd	**2-py** exp	**2-py** calcd
Mo−Mo (Å)	2.1112(4)	2.1077	2.1356(3)	2.1664
Mo−N avg (Å)	2.145[2]	2.1325	2.119[2]	2.1234
Mo−S avg (Å)	2.4753[8]	2.4965	2.5172[6]	2.5192
Mo−Li (Å)			3.075(5)	3.0430
Mo−Cl (Å)			2.6533(6)	2.5066
S−Mo−S avg (deg)	168.30[2]	165.16	169.60[5]	172.56
N−Mo−N avg (deg)	168.19[6]	168.40	166.7[1]	163.92

structure values. For compound **1a**, the calculated structure accurately reproduces the crystal structure geometry. The calculated Mo−Mo bond distance of 2.1077 Å only differs by 0.0035 Å from the crystal structure value of 2.1112(4) Å. The Mo−Mo bond distance calculated here corresponds to a Mayer bond order of 3.3, slightly less than the idealized value of 4. The average Mo−N and Mo−S bond distances differ minimally from the crystal structure values. The calculated N−Mo−N bond angle is very close to the crystal structure value, but there is a more significant difference between the calculated S−Mo−S bond angle and the crystal structure value [Δ(N−Mo−N) = 0.21°; Δ(S−Mo−S) = 3.18°].

For compound **2-py**, the calculated model adequately reproduces how the equatorial ligands bind to the Mo_2 core, as shown by how well the calculated Mo−N and Mo−S bond distances agree with the crystal structure values, but the axial Mo−Cl bond distance is significantly underestimated by ∼0.15 Å. However, the potential energy surface (PES) for stretching of the Mo−Cl bond (SI, Figure S1) indicates that elongating the Mo−Cl bond to the experimental value only increases the total energy by ∼5 kJ mol^{-1}, which can be caused by crystal packing effects. It should be noted, though, that increasing the Mo−Cl distance to a "normal" value, above 2.8 Å, incurs a greater energetic penalty (>14 kJ mol^{-1}). Thus, the DFT results clearly indicate stabilization of an unusually short Mo−Cl bond in **2-py**.

Single-point calculations performed on the optimized structures of **1a** and **2-py** give insight into their electronic structures. MO diagrams based on the DFT results for the metal−metal bonding orbitals of **1a** and **2-py** are shown in Figure 8. The metal−metal bonding orbitals are the most

dx.doi.org/10.1021/ic400275x | Inorg. Chem. 2013, 52, 4658−4667

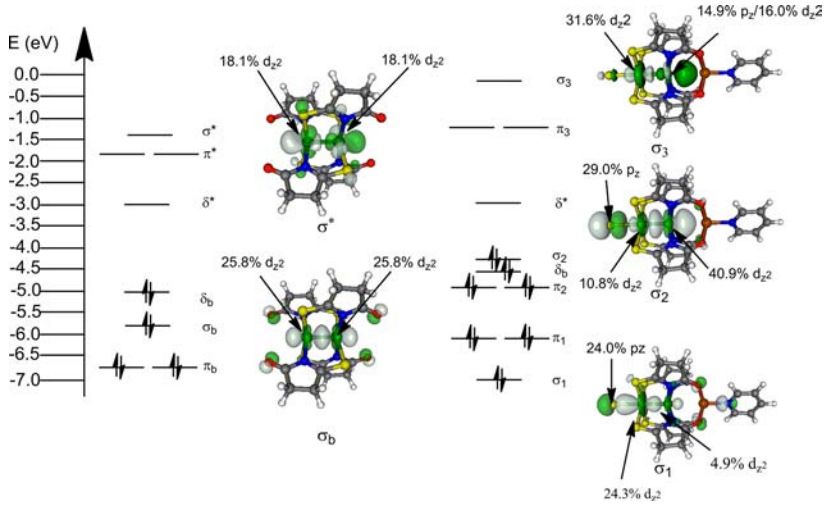

Figure 8. MO diagrams of compounds **1a** and **2-py**. Only the orbitals with significant contributions from the Mo atoms are shown. The percent contributions of the major components of the σ-type orbitals are indicated next to the diagram of those orbitals.

important orbitals because they govern how these complexes interact with the axial Li^+ ion and Cl^- ion. For **1a**, the MO diagram shows a deviation from the predicted qualitative MO diagram shown in Chart 1 in that the Mo−Mo π-bonding orbitals are lower in energy than the Mo−Mo σ-bonding orbital, which is raised in energy because of antibonding interactions with the SNO5 ligand. As expected, the highest occupied MO (HOMO) is a Mo−Mo δ-bonding orbital, and the lowest unoccupied MO (LUMO) is a Mo−Mo δ-antibonding orbital, as predicted by the qualitative MO diagram.

For compound **2-py**, the HOMO is a σ-type orbital (σ_2; Figure 8) rather than a δ-type orbital, which is a major deviation from the predicted qualitative MO diagram in Chart 1. Elevation of the σ_2 orbital to HOMO over the δ-type orbital results from interaction of the Mo_2 core with the axial Cl^-, as shown in Scheme 3. If we take the Mo−Mo−Cl vector to be the z axis, then the Cl p_z lone-pair orbital is energetically well situated to interact with the filled Mo_2 σ orbital, with which it forms a bonding (σ_1) and antibonding (σ_2) combination. The Mo_2 σ^* orbital also mixes with the Cl p_z and Mo_2 σ, yielding σ_3, which is antibonding with respect to both the Mo−Mo and Mo−Cl interactions. Thus, the two Mo atoms and the Cl^- ligand form something akin to a 3-center 4-electron σ bond. The σ_2 orbital is elevated in energy to become the HOMO, while the σ_1 orbital is brought down in energy by the interaction.

Scheme 3. Qualitative MO Diagram Illustrating the Origin of the σ-Type Orbitals in 2-py

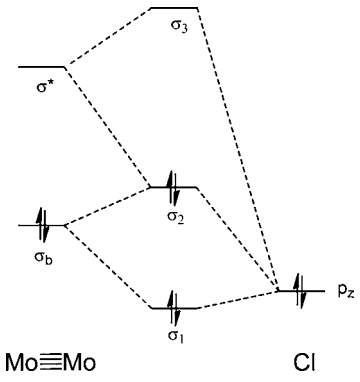

The most striking difference between the MO diagrams of compounds **1a** and **2-py** is shown in polarization of the σ-type orbitals in **2-py** compared with **1a**. In compound **1a**, each σ-type MO has a 50% contribution from each Mo atom. However, in **2-py**, the orbitals are not evenly distributed. In the σ_1 orbital, the MO is polarized 4.96:1 toward the Mo atom directly bound to the Cl^-, and in the σ_2 orbital, the MO is polarized 3.79:1 toward the Mo atom closest to Li^+. This polarization is due to the interaction of Li^+ and Cl^- with Mo_2 and, to a lesser extent, the 4,0 disposition of the SNO ligands, but the individual contribution of Li^+ cannot be determined by this MO diagram alone.

Geometry optimization and single-point calculations were also performed on $[pyLiMo_2(SNO5)_4]^+$, which is **2-py** from which the Cl^- ligand has been removed. The σ^* and σ_b orbitals are the primary orbitals with which a σ-type orbital on Cl^- will interact when forming an axial Mo−Cl bond. In the σ^* orbital shown in Figure 9, the orbital is polarized toward the open axial position by significant mixing of the Mo $5p_z$ orbital with the

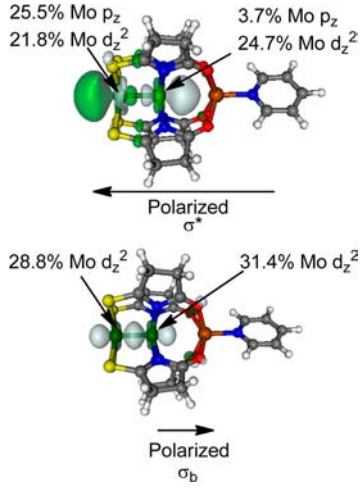

Figure 9. σ^* and σ_b orbitals of $[pyLiMo_2(SNO5)_4]^+$ showing polarization caused by the presence of Li^+.

dx.doi.org/10.1021/ic400275x | Inorg. Chem. 2013, 52, 4658−4667

$4d_{z^2}$ orbital of the exposed axial Mo atom. This polarization makes the σ^* orbital much more available to interact with a Cl^- σ-type orbital. In the σ_b orbital, the polarization is less pronounced because it is too low in energy to mix with the $5p_z$ orbital. As a result of polarization of these orbitals, the Cl^- ligand forms a much stronger bond with the Mo_2 core of **2-py** than in unactivated Mo_2Cl complexes.

CONCLUSIONS

Cationic lithium has been successfully shown by X-ray crystallography to activate an axial site of a Mo_2 complex. The activated compound was shown to thermodynamically favor lithium binding, which is reversible in coordinating solvents. DFT calculations on these compounds gave geometries in close agreement with experiment, and they provided an electronic explanation for the increased affinity of Mo_2 for the axial Cl^- ligand in a Lewis acid activated complex. The Lewis acid activation results from polarization of the MOs and subsequent strengthening of the Mo−Cl bond, as evidenced by the X-ray crystal data and DFT calculations. On the basis of the data shown here, it is possible that these compounds could also find utility as Li^+ ion sensors.

ASSOCIATED CONTENT

Supporting Information

Crystallographic data in CIF format and computed PES for the Mo−Cl bond in **2-py**. This material is available free of charge via the Internet at http://pubs.acs.org.

AUTHOR INFORMATION

Corresponding Author

*E-mail: berry@chem.wisc.edu.

Notes

The authors declare no competing financial interest.

ACKNOWLEDGMENTS

The authors acknowledge financial support from the National Science Foundation under Grants CHE-0745500, CHE-9208463 (Bruker AC 360), and CHE-0840494 (computational facilities) and a generous bequest from Paul J. Bender (Bruker Avance 500).

REFERENCES

(1) *Multiple Bonds between Metal Atoms*, 3rd ed.; Cotton, F. A., Murillo, C. A., Walton, R. A., Eds.; Springer Science and Business Media: New York, 2005.

(2) (a) Kornecki, K. P.; Powers, D. C.; Ritter, T.; Berry, J. F. submitted for publication. (b) Berry, J. F. *Dalton Trans.* **2012**, *41*, 700−713. (c) Davies, H. M. L.; Manning, J. R. *Nature* **2008**, *451*, 417−424. (d) DuBois, J. *Org. Process Res. Dev.* **2011**, *15*, 758−762. (e) Doyle, M. P.; Duffy, R.; Ratnikov, M.; Zhou, L. *Chem. Rev.* **2010**, *110*, 704−724. (f) Powers, D. C.; Ritter, T. *Acc. Chem. Res.* **2012**, *45*, 840−850. (g) Villalobos, L.; Cao, Z.; Fanwick, P. E.; Ren, T. *Dalton Trans.* **2012**, *41*, 644−650. (h) Teets, T. S.; Nocera, D. G. *Chem. Commun.* **2011**, *47*, 9268−9274.

(3) (a) Chisholm, M. H. *Macromol. Chem. Phys.* **2012**, *213*, 800−807. (b) Chisholm, M. H.; Lear, B. J. *Chem. Soc. Rev.* **2011**, *40*, 5254−5265. (c) Alberding, B. G.; Chisholm, M. H.; Gallucii, J. C.; Ghosh, Y.; Gustafson, T. L. *Proc. Natl. Acad. Sci. U.S.A.* **2011**, *108*, 8152−8156. (d) Bradley, P. M.; Fu, P. K.-L.; Turro, C. *Comments Inorg. Chem.* **2001**, *22*, 393−426.

(4) (a) Chisholm, M. H. *Struct. Bonding (Berlin)* **2010**, *136*, 29. (b) Chisholm, M. H.; Patmore, N. S. *Acc. Chem. Res.* **2007**, *40*, 19−27. (c) Berry, J. F. *Struct. Bonding (Berlin)* **2010**, *136*, 1. (d) Mohan, P. J.; Georgiev, V. P.; McGrady, J. E. *Chem. Sci.* **2012**, *3*, 1319−1329. (e) Manni, G. L.; Dzubak, A. L.; Mulla, A.; Brogden, D. W.; Berry, J. F.; Gagliardi, L. *Chem.—Eur. J.* **2012**, *18*, 1737−1749.

(5) (a) Chisholm, M. H.; Macintosh, A. M. *Chem. Rev.* **2005**, *105*, 2949−2976. (b) Cotton, F. A.; Lin, C.; Murillo, C. A. *Acc. Chem. Res.* **2001**, *34*, 759−771. (c) Filatov, A. S.; Napier, M.; Vreshch, V. D.; Sumner, N. J.; Dikarev, E. V.; Petrukhina, M. A. *Inorg. Chem.* **2012**, *51*, 566−571. (d) Filatov, A. S.; Petrukhina, M. A. *Coord. Chem. Rev.* **2010**, *254*, 2234−2246.

(6) (a) Nippe, M.; Timmer, G. H.; Berry, J. F. *Chem. Commun.* **2009**, 4357−4359. (b) Nippe, M.; Victor, E.; Berry, J. F. *Inorg. Chem.* **2009**, *48*, 11889−11895. (c) Long, A. K. M.; Yu, R. P.; Timmer, G. H.; Berry, J. F. *J. Am. Chem. Soc.* **2010**, *132*, 12228−12230. (d) Nippe, M.; Goodman, S. M.; Fry, C. G.; Berry, J. F. *J. Am. Chem. Soc.* **2011**, *133*, 2856−2859. (e) Long, A. K. M.; Timmer, G. H.; Pap, J. S.; Snyder, J. L.; Yu, R. P.; Berry, J. F. *J. Am. Chem. Soc.* **2011**, *133*, 13138−13150. (f) Nippe, M.; Turov, Y.; Berry, J. F. *Inorg. Chem.* **2011**, *50*, 10592−10599. (g) Turov, Y.; Berry, J. F. *Dalton Trans.* **2012**, *41*, 8153−8161. (h) Timmer, G. H.; Berry, J. F. *Chem. Sci.* **2012**, *3*, 3038−3052.

(7) (a) Cotton, F. A.; Ilsley, W. H.; Kaim, W. *Inorg. Chem.* **1980**, *19*, 3586−3589. (b) Cotton, F. A.; Favello, L. R.; Han, S.; Wang, W. *Inorg. Chem.* **1983**, *22*, 4106−4112. (c) Cayton, R. H.; Chisholm, M. H.; Huffman, J. C.; Lobkovsky, E. B. *J. Am. Chem. Soc.* **1991**, *113*, 8709−8724. (d) Pimblett, G.; Garner, C. D.; Clegg, W. *J. Chem. Soc., Dalton Trans.* **1986**, 1257−1263. (e) Clegg, W.; Pimblett, G.; Garner, C. D. *Polyhedron* **1986**, *5*, 31−33. (f) Cotton, F. A.; Reid, A. H., Jr.; Schwotzer, W. *Inorg. Chem.* **1985**, *24*, 3965−3968. (g) Cotton, F. A.; Kühn, F. E. *Inorg. Chim. Acta* **1996**, *252*, 257−264. (h) Cotton, F. A.; Daniels, L. M.; Murillo, C. A.; Wang, X. *Polyhedron* **1998**, *17*, 2781−2793. (i) Day, E. F.; Huffman, J. C.; Folting, K.; Christou, G. *J. Chem. Soc., Dalton Trans.* **1997**, 2837−2841. (j) Cotton, F. A.; Wiesinger, K. J. *Inorg. Chem.* **1991**, *30*, 871−873. (k) Xue, W.-M.; Kühn, F. E.; Zhang, G.; Herdtweck, E.; Raudaschl-Sieber, G. *J. Chem. Soc., Dalton Trans.* **1999**, 4103−4110. (l) Kuang, S.-M.; Fanwick, P. E.; Walton, R. A. *Inorg. Chim. Acta* **2000**, *305*, 102−105.

(8) (a) Robbins, G. A.; Martin, D. S. *Inorg. Chem.* **1984**, *23*, 2086−2093. (b) Wu, Y.-Y.; Chen, J.-D.; Liou, L.-S.; Wang, J.-C. *Inorg. Chim. Acta* **1997**, *258*, 193−199. (c) Suen, M.-W.; Tseng, G.-W.; Chen, J.-D.; Keng, T.-C.; Wang, J.-C. *Chem. Commun.* **1999**, 1185−1186. (d) Udovic, B.; Leban, I.; Segedin, P. *Croat. Chem. Acta* **1999**, *72*, 477−499. (e) Yi, J.; Miyabayashi, T.; Ohashi, M.; Yamagata, T.; Mashima, K. *Inorg. Chem.* **2004**, *43*, 6596−6599. (f) Arnold, D. I.; Cotton, F. A.; Kühn, F. E. *Inorg. Chem.* **1996**, *35*, 4733−4737. (g) Nippe, M.; Bill, E.; Berry, J. F. *Inorg. Chem.* **2011**, *50*, 7650−7661. (h) Nippe, M.; Victor, E.; Berry, J. F. *Eur. J. Inorg. Chem.* **2008**, 5569−5572. (i) Cotton, F. A.; Fanwick, P. E. *Inorg. Chem.* **1983**, *22*, 1327−1332.

(9) Cotton, F. A.; Mester, Z. C.; Webb, T. R. *Acta Crystallogr.* **1970**, *B30*, 2768−2770.

(10) (a) Gabbaï, F. P.; Schier, A.; Riede, J.; Sladek, A.; Görlitzer, H. W. *Inorg. Chem.* **1997**, *36*, 5694−5698. (b) Wade, C. R.; Lin, T.-P.; Nelson, R. C.; Mader, E. A.; Miller, J. T.; Gabbaï, F. P. *J. Am. Chem. Soc.* **2011**, *133*, 8948−8955. (c) Lin, T.-P.; Nelson, R. C.; Wu, T.; Miller, J. T.; Gabbaï, F. P. *Chem. Sci.* **2012**, *3*, 1128−1136.

(11) (a) Greenwood, B. P.; Forman, S. I.; Rowe, G. T.; Chen, C.-H.; Foxman, B. M.; Thomas, C. M. *Inorg. Chem.* **2009**, *48*, 6251−6260. (b) Krogman, J. P.; Foxman, B. M.; Thomas, C. M. *J. Am. Chem. Soc.* **2011**, *133*, 14582−14585.

(12) (a) Ferguson, G. S.; Wolczanski, P. T. *Organometallics* **1985**, *4*, 1601−1605. (b) Ferguson, G. S.; Wolczanski, P. T. *J. Am. Chem. Soc.* **1986**, *108*, 8293−8295. (c) Ferguson, G. S.; Wolczanski, P. T.; Párkányi, L.; Zonnevylle, M. C. *Organometallics* **1988**, *7*, 1967−1979. (d) Baxter, S. M.; Ferguson, G. S.; Wolczanski, P. T. *J. Am. Chem. Soc.* **1988**, *110*, 4231−4241.

(13) (a) Nagashima, H.; Sue, T.; Oda, T.; Kanemitsu, A.; Matsumoto, T.; Motoyama, Y.; Sunada, Y. *Organometallics* **2006**, *25*, 1987−1994. (b) Sunada, Y.; Sue, T.; Matsumoto, T.; Nagashima, H. *J. Organomet. Chem.* **2006**, *691*, 3176−3182. (c) Sue, T.; Sunada, Y.; Nagashima, H. *Eur. J. Inorg. Chem.* **2007**, 2897−2908. (d) Tsutsumi,

H.; Sunada, Y.; Shiota, Y.; Yoshizawa, K.; Nagashima, H. *Organometallics* **2009**, *28*, 1988−1991.
(14) Scott, T. A.; Abbaoui, B.; Zhou, H.-C. *Inorg. Chem.* **2004**, *43*, 2459−2461.
(15) Holste, G.; Schäfer, H. *Z. Anorg. Allg. Chem.* **1972**, *391*, 263−270.
(16) Cotton, F. A.; Norman, J. G. *J. Coord. Chem.* **1971**, *1*, 161−172.
(17) Berg, U.; Sandström, J. *Acta Chem. Scand.* **1966**, *20*, 689−697.
(18) Zhu, X.; Giordano, T.; Yu, Q.-S.; Holloway, H. W.; Perry, T. A.; Lahiri, D. K.; Brossi, A.; Greig, N. H. *J. Med. Chem.* **2003**, *46*, 5222−5229.
(19) (a) *SMART*; Bruker-AXS: Madison, WI, 2009. (b) Sheldrick, G. M. *Acta Crystallogr.* **2008**, *A64*, 112−122. (c) Dolomanov, O. V.; Bourhis, L. J.; Gildea, R. J.; Howard, J. A. K.; Puschmann, H. *J. Appl. Cryst.* **2009**, *42*, 339−341.
(20) Flack, H. D. *Acta Crystallogr.* **1983**, *A39*, 876−881.
(21) (a) Neese, F. *ORCA—An ab Initio DFT and Semi-empirical Electronic Structure Package*, version 2.8.0; University of Bonn: Bonn, Germany, 2010. (b) Perdew, J. P. *Phys. Rev. B: Condens. Matter* **1986**, *33*, 8822−8824. (c) Becke, A. D. *Phys. Rev. A: At., Mol., Opt. Phys.* **1988**, *38*, 3098−3100.
(22) Weigend, F.; Ahlrichs, R. *Phys. Chem. Chem. Phys.* **2005**, *7*, 3297−3305.
(23) Crystals of $LiMo_2(SNO6)_4Cl$ were obtained, and the linear Mo≣Mo···Li structure was determined by crystallographic characterization. Crystallographic data are monoclinic, *Cc*, a = 14.9958(5) Å, b = 11.1604(4) Å, c = 18.4996(7) Å, β = 108.995(2)°, and V = 2927.5(2) Å^3. The Mo≣Mo and Mo−Cl distances are 2.135(1) and 2.715(2) Å, respectively.
(24) (a) Cotton, F. A.; Niswander, R. H.; Sekutowski, J. C. *Inorg. Chem.* **1979**, *18*, 1149−1151. (b) Ambrosius, H. P. M. M.; Cotton, F. A.; Falvello, L. R.; Hintzen, H. T. J. M.; Melton, T. J.; Schwotzer, W.; Tomas, M.; van der Linden, J. G. M. *Inorg. Chem.* **1984**, *23*, 1611−1616. (c) Fanwick, P. E.; Qi, J.-S.; Wu, Y.-P.; Walton, R. A. *Inorg. Chim. Acta* **1990**, *168*, 159−161. (d) Sheldrick, W. S.; Mintert, M. *Inorg. Chim. Acta* **1994**, *219*, 23−29. (e) Hicks, J.; Ring, S. P.; Patmore, N. J. *Dalton Trans.* **2012**, *41*, 6641−6650.
(25) (a) Bailey, P. J.; Bone, S. F.; Mitchell, L. A.; Parsons, S.; Taylor, K. J.; Yellowlees, L. J. *Inorg. Chem.* **1997**, *36*, 867−871. (b) Bailey, P. J.; Bone, S. F.; Mitchell, L. A.; Parsons, S.; Taylor, K. J.; Yellowlees, L. J. *Inorg. Chem.* **1997**, *36*, 5420. (c) Cotton, F. A.; Daniels, L. M.; Hillard, E. A.; Murillo, C. A. *Inorg. Chem.* **2002**, *41*, 1639−1644. (d) Lin, C.; Protasiewicz, J. D.; Smith, E. T.; Ren, T. *Inorg. Chem.* **1996**, *35*, 6422−6428. (e) Cotton, F. A.; Daniels, L. M.; Murillo, C. A.; Timmons, D. J.; Wilkinson, C. C. *J. Am. Chem. Soc.* **2002**, *124*, 9249−9256. (f) Chisholm, M. H.; D'Acchioli, J. S.; Pate, B. D.; Patmore, N. J.; Dalal, N. S.; Zipse, D. J. *Inorg. Chem.* **2005**, *44*, 1061−1067.
(26) (a) Fukuzumi, S.; Ohkubo, K. *Coord. Chem. Rev.* **2010**, *254*, 372−385. (b) Fukuzumi, S.; Ohkubo, K.; Morimoto, Y. *Phys. Chem. Chem. Phys.* **2012**, *14*, 8472−8484.
(27) (a) Yokota, Y.; Young, V. G., Jr.; Verkade, J. G. *Acta Crystallogr.* **1999**, *C55*, 196−198. (b) Seo, D. M.; Boyle, P. D.; Henderson, W. A. *Acta Crystallogr.* **2011**, *E67*, m1148.
(28) Danil de Namor, A. F.; Ng, J. C. Y.; Tanco, M. A. L.; Salomon, M. *J. Phys. Chem.* **1996**, *100*, 14485−14491.

dx.doi.org/10.1021/ic400275x | *Inorg. Chem.* 2013, 52, 4658−4667